

The PG X-ray QSO sample: Links between the UV-X-ray Continuum and Emission Lines

Beverley J. Wills¹, M. S. Brotherton², A. Laor³, D. Wills¹, B. J. Wilkes⁴, G. J. Ferland⁵, & Zhaohui Shang¹

Abstract.

The UV to soft X-rays of luminous AGNs dominate their bolometric luminosity, driven by an accretion-powered dynamo at the center. These photons ionize the surrounding gas, thereby providing clues to fueling and exhaust. Two sets of important relationships – neither of them understood – link the continuum and gas properties.

(i) Boroson & Green's 'eigenvector 1' relationships: Steeper soft X-ray spectra are clearly related to narrower H β emission and stronger optical Fe II emission from the BLR, and weaker [O III] λ 5007 from the NLR. We show that these relationships extend to UV spectra: narrower C III] λ 1909, stronger low ionization lines, larger Si III] λ 1892/C III] λ 1909 (a density indicator), weaker C IV λ 1549 but stronger higher-ionization N V λ 1240. We speculate that high accretion rates are linked to high columns of dense ($10^{10} - 10^{11}$ cm $^{-3}$), nitrogen-enhanced, low-ionization gas from nuclear starbursts. Linewidth, inverse Fe II-[O III] and inverse Fe II-C IV relationships hint at the geometrical arrangement of this gas.

(ii) The Baldwin effect (inverse equivalent width – luminosity relationships): Our correlation analyses suggest that these are independent of the above eigenvector 1 relationships. The eigenvector 1 relationships can therefore be used in future work, to reduce scatter in the Baldwin relationships, perhaps fulfilling the dream of using the Baldwin effect for cosmological studies.

1. Introduction

The UV to soft X-rays of luminous AGNs dominate their bolometric luminosity, driven by an accretion-powered dynamo at the center. Reprocessing of energy within a few gravitational radii determines the spectral energy distribution at

¹McDonald Observatory & Astronomy Department, University of Texas at Austin, TX 78712, USA

²Institute of Geophysics & Planetary Physics, Lawrence Livermore National Laboratory, Livermore, CA 94550, USA

³Department of Physics, Technion, Israel Institute of Technology, Haifa 32000, Israel

⁴Center for Astrophysics, 60 Garden Street, Cambridge MA 02138, USA

⁵University of Kentucky, Department of Physics and Astronomy, Lexington, KY 40506, USA

optical photon energies and above. These photons illuminate and ionize the surrounding gas on sub-parsec to kiloparsec scales – the fuel and exhaust of the central engine – enabling us to investigate its structure, dynamics and physical conditions.

Echo-mapping and photoionization modeling shows that luminous QSOs' strong broad emission lines arise within 1 pc of the ionizing continuum, from gas with a range of distances, velocities ($1000 \text{ km s}^{-1} - 10,000 \text{ km s}^{-1}$), densities (at least $10^9 \text{ cm}^{-3} - 10^{12} \text{ cm}^{-3}$), and optical depths. This is the broad line region (BLR). Its average line strengths can be reproduced quite well (the “locally optimally emitting cloud” model of Baldwin et al. 1995; see Korista’s discussion in this volume). Beyond the BLR, at distances up to many kiloparsecs, is lower density and lower velocity ($\sim 500 \text{ km s}^{-1}$) gas of the narrow line region (NLR).

Because QSO spectra are similar, the emphasis until recently, has been on explaining the average QSO spectrum. However, investigating *relationships* among QSO spectral parameters (absorption and emission) as a function of the properties of the ionizing continuum is a powerful way to further explore how the central dynamo works (Francis et al. 1992).

There are two important sets of relationships linking central engine properties with the surrounding gas – the Baldwin effect in the UV (Baldwin et al. 1978), and the optical–X-ray “eigenvector 1” relationships first clearly presented by Boroson & Green (1992).

The Baldwin effect is an inverse relationship between QSO luminosity and the equivalent width (EW) of CIV $\lambda 1549$ (Baldwin et al. 1978), and other broad emission lines (Kinney et al. 1990). Because QSOs are exceedingly luminous and therefore visible at high redshifts, EWs could serve to determine luminosity distances. QSOs could then be a tool for cosmology. This hope has not been fulfilled because there is too much scatter in the Baldwin relationships.

In optical QSO samples, much of the spectrum-to-spectrum variation is explained by the strong eigenvector 1 relationships (hereafter called principal component 1 or PC1): As H β from the BLR becomes narrower, the strength of BLR Fe II (optical) emission increases, [O III] NLR emission decreases, and the optical–X-ray and X-ray spectra steepen (increasing α_{ox} and α_x , where $F_\nu \propto \nu^{-\alpha}$) (Boroson & Green 1992, Laor et al. 1994, 1997a, Grupe et al. 1998). These relationships link the emission-line properties to the central engine:

- The UV to soft X-ray region dominates the radiated power and ionizes the BLR.
- In principle, line widths (profiles), together with BLR distances based on echo-mapping time-delays or dust-sublimation radii, may be used to infer the virial central masses, hence L_{Edd} (Peterson et al. 1998, Laor 1998). QSO luminosities often appear to be significant compared with L_{Edd} , suggesting that accretion onto a central Black Hole could be an unstable process, giving rise to winds.
- Line widths are also related to α_x , linking kinematics directly to a central engine property. By analogy with Galactic Black Hole Candidates in their “high” states, steep X-ray spectra may be related to high accretion rates (Pounds, Done, & Osborne 1995).
- The structure of the BLR must be linked to α_x and hence probably to accretion and outflowing winds. One possible explanation for the inverse Fe II-[OIII] relation is that the smaller the effective covering of the central engine by opti-

cally thick BLR gas, the more photons are available to ionize the more distant NLR (Boroson & Green 1992, Brotherton, this volume).

- Clues to the geometry may also come from the fact that the BLR appears to see more continuum power than we infer from the observed continuum; there are too few ionizing photons to explain the line strengths – especially low ionization lines like Fe II, but also He II $\lambda 1640$ (Netzer 1985, Korista et al. 1997).

Here we present new UV relationships linking QSOs' spectral energy distribution and the kinematics, structure and physical properties of the emitting gas. We show how these relationships could be used to reduce the scatter in the Baldwin relationship and lead to understanding of the effect itself.

We have investigated the UV spectra of 22 QSOs¹ from the complete, optically selected sample of 23 QSOs with complete and high quality ROSAT (0.15 - 2 keV) spectroscopy (Laor et al. 1994). This is the same sample for which Laor et al. (1994, 1997a) showed striking X-ray-optical PC1 relationships. A briefer report of the present work appeared in Wills et al. (1998a).

2. Observations & Measurements

We have obtained HST FOS spectrophotometry from wavelengths below Ly α to beyond the atmospheric cut-off, and McDonald Observatory spectrophotometry from the atmospheric cut-off to beyond H α . Instrumental resolutions range from 230 – 350 km s $^{-1}$ (FWHM). Here we emphasize the new results from UV spectroscopy, with most optical data taken from Boroson & Green (1992). In Figure 1 we show sample UV spectra, with QSOs arranged from the bottom in order of increasing optical PC1, in the sense of steeper soft X-ray spectrum and increasing strength of Fe II(optical).

We have measured strengths, ratios and widths (FWHM) for the following emission lines of the BLR: We have deblended Ly α and N V $\lambda 1240$ from each other and from Si II $\lambda 1260$, O I $\lambda 1304$ and C II $\lambda 1335$. We measured C IV $\lambda 1549$ with N IV $\lambda 1486$, He II $\lambda 1640$ and [O III] $\lambda 1663$ removed, and we have deblended Al III $\lambda 1860$, Si III] $\lambda 1892$ and C III] $\lambda 1909$. In most cases we used our McDonald spectra to define a 'rest frame' wavelength scale referred to [O III] $\lambda 5007$ from the NLR. The $\lambda 1909$ feature is a blend of Si III $\lambda 1892$, C III] $\lambda 1909$ and Fe III lines. For our sample Fe III is a minor contributor. Evidence for this is that the wavelength of the peak corresponds to within 0.5-1 Å rms of the expected wavelength of C III] $\lambda 1909$. An exception is Mkn 478, where Fe III is a clearly present. We have deblended the Ly α -N V emission lines in several ways, some assuming the N V components to have the same width as Ly α , and others assuming the same width as the components of C IV $\lambda 1549$, with qualitatively similar results. The greatest uncertainties in line measurements arise from uncertainties in continuum placement, and in removal of associated and Galactic interstellar absorption. Details will be presented by Wills et al. (1998b). Some actual line measurements are tabulated by Francis & Wills (this volume).

¹One object was omitted for non-scientific reasons, so this omission does not bias the sample.

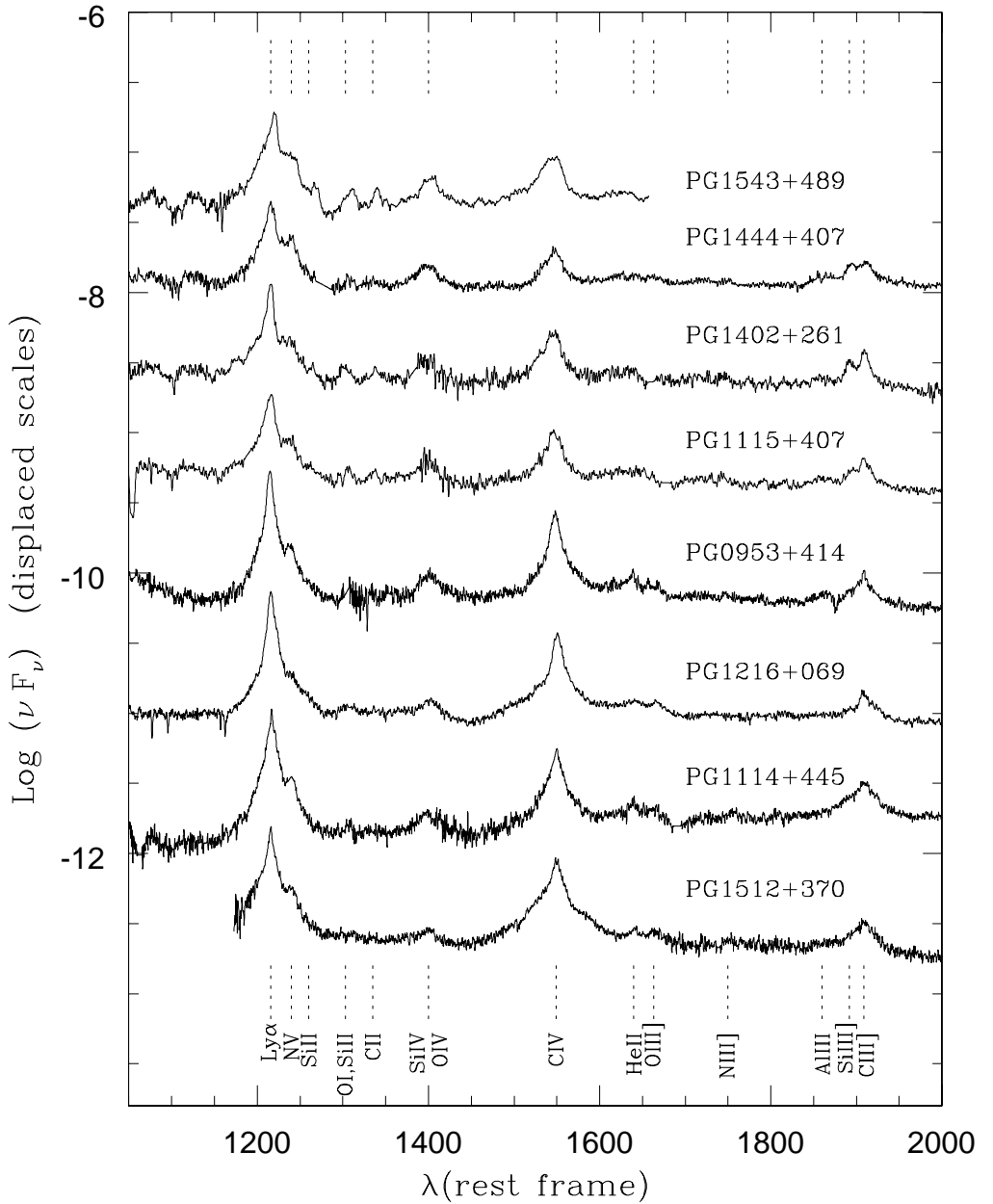


Figure 1. HST-FOS spectra of PG QSOs, plotted on a logarithmic flux density scale to emphasize the weaker features. They are plotted in order of PC1, with the 3 lower QSOs having amongst the flattest X-ray spectra (smaller α_x) and weakest Fe II(optical)), and the 3 top spectra being those QSOs with softest X-ray spectra, strongest optical Fe II(optical), weaker [OIII] $\lambda 5007$, and narrowest (BLR) H β . Increasing upwards, notice the increasing prominence of AlIII $\lambda 1860$, SiIII $\lambda 1892$, OI $\lambda 1304$, C II $\lambda 1335$. The $\lambda 1400$ blend of O IV] and Si IV, as well as the apparent strength of NV $\lambda 1240$ increase relative to C IV and Ly α . The strength of the optical and UV Fe II blends (not shown) also increases.

3. Correlation Results

3.1. Direct Correlations

Table 1. Some Correlation Coefficients^a

UV Parameters	Optical First Principal Component Parameters						L ₁₂₁₆
	α_x	log FW	log EW	Fe II/	log EW	opt-Xray	
	H β	Fe II	H β	[O III]	PC1		
log FW C III]	-0.60	+0.78	-0.49	-0.52	+0.21	-0.57	+0.18
log EW Ly α	-0.13	+0.27	-0.02	-0.16	+0.34	-0.17	-0.77
log EW C IV	-0.49	+0.69	-0.53	-0.62	+0.67	-0.68	-0.39
C IV/Ly α	-0.61	+0.68	-0.67	-0.67	+0.59	-0.77	+0.08
log EW C III]	-0.32	+0.42	-0.18	-0.36	+0.41	-0.34	-0.68
Si III]/C III]	+0.52	-0.56	+0.52	+0.89	-0.62	+0.62	-0.10
Si III/Ly α	+0.39	-0.59	+0.57	+0.83	-0.70	+0.72	-0.22
N V/C III]	+0.71	-0.53	+0.47	+0.65	-0.51	+0.73	+0.08
N V/Ly α	+0.53	-0.48	+0.41	+0.45	-0.57	+0.66	-0.01
λ 1400/Ly α	+0.69	-0.60	+0.60	+0.58	-0.57	+0.71	-0.31

^aThe usual Pearson correlation coefficients are given.

For 22 QSOs, a correlation coefficient of 0.4 corresponds to 1 chance in 15 of arising from uncorrelated variables (two tailed), 0.5 corresponds to 1 chance in 50, 0.6 to 1 chance in 300, and 0.7 to 1 chance in 2000 of arising from uncorrelated variables. FW \equiv FWHM.

Some of the most important correlation results are summarized in Table 1 and Figure 2. Column (1) of Table 1 lists emission-line parameters of the ultraviolet spectrum: line ratios, logarithms of rest-frame equivalent widths (EW) and line widths (full width at half maximum, FWHM or FW). Columns (2) – (6) give correlation coefficients for the ultraviolet parameters vs. the well-known PC1 parameters, α_x derived from a fit between 0.2 keV and 2 keV, and parameters of the optical spectrum as given by Boroson & Green (1992). Column (7) gives correlation coefficients between the UV parameters of col. (1) and a linear combination of X-ray-optical PC1 parameters derived from a principal components analysis of our sample (See §3.2 and Francis & Wills, this volume). The table notes give two-tailed significance levels for the correlation coefficients. Where the probability of a correlation arising by chance from unrelated variables is <1 in 50, the coefficients are given in bold type. However, because such a large fraction of our observationally-independent parameters are significantly correlated, the assumption that the variables are unrelated breaks down, so the significance of our correlations is actually higher than indicated in the table. Figure 2 plots some of the correlations of Table 1, the four columns representing X-ray-optical PC1 observables: the steepness of the X-ray spectrum, the width of the broad H β line, the strength of Fe II(optical), and the strength of NLR emission ([O III] λ 5007). Optical PC1, in the sense of softer X-ray spec-

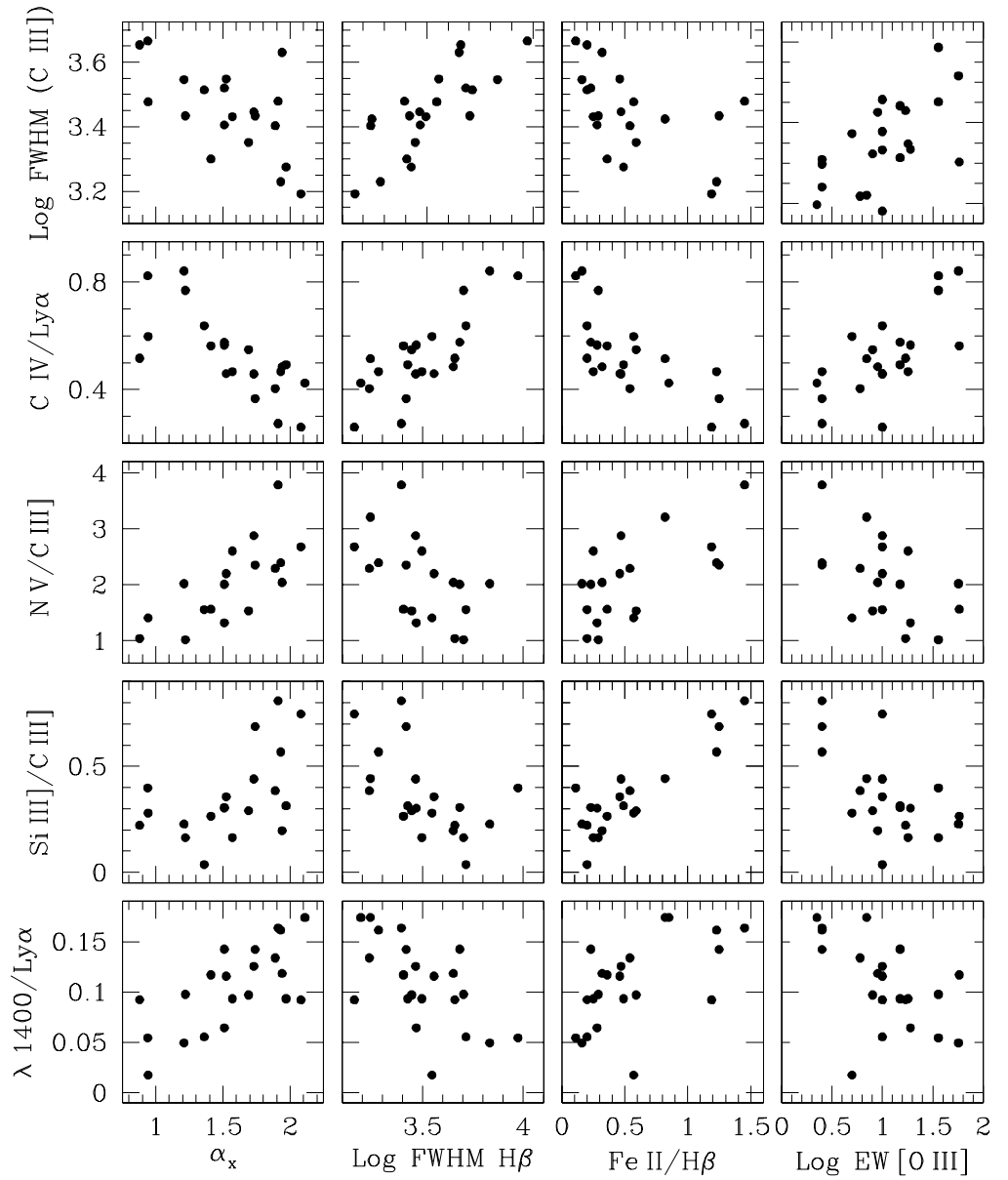


Figure 2. UV observables vs. α_x and optical Eigenvector 1 observables. Many line ratios are consistent with these trends – lower ionization, higher densities, in addition to (not shown) weaker [O III] $\lambda 5007$ from the narrow line region (NLR) – all corresponding to steeper soft X-ray spectra. The 2-tailed probability of these correlations arising by chance from unrelated variables is between 1 in 50 to 1 in $\gg 1000$.

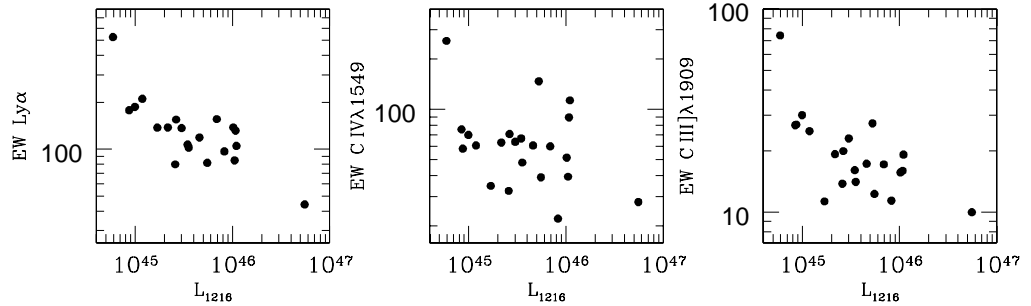


Figure 3. The Baldwin relationships for Ly α , C IV λ 1549 and C III] λ 1909 for \sim 20 QSOs of the PG X-ray sample.

trum, clearly extends to the UV: narrower C III] emission, stronger N V λ 1240, Si III] λ 1892, and λ 1400 feature. Fe III UV 34 ($\lambda\lambda$ 1895, 1914, 1926) also contributes more when Fe II is strong. Mkn 478 in our sample, and I Zw 1 (see Laor et al. 1997b), have especially soft X-ray spectra, especially strong Fe II(optical), as well as strong Fe III (I Zw 1 did not meet the Galactic obscuration criteria for inclusion in the sample, but is otherwise eligible). The strength of C IV λ 1549 is inversely correlated with the strength of Fe II (optical) (Wang et al. 1996) and correlated with [O III] (Brotherton, this volume.) There are also very significant correlations among the UV parameters by themselves (§3.2). Correlations as strong as we have found should show up in a visual inspection of the spectra. They do (see Figure 1, being careful to account for the effects of line width on blended features).

Also shown in Table 1 and Fig. 3 are correlations between UV emission-line parameters and L_{1216} , log of the continuum luminosity at 1216 \AA . The Baldwin relationships are present. The significance depends largely on the highest luminosity QSO 3C 273 with the smallest EWs, and the lowest luminosity QSO PG 1202+281 with the largest EWs. A larger sample is needed to show this result clearly.

3.2. Principal Components Analysis

We perform a principal components analysis (PCA) to investigate which sets of observational variables correlate or anticorrelate together, and therefore whether we can define a smaller number of new variables that are linear combinations of the measured variables. This would simplify a description of our dataset. Moreover, it may suggest one or more physical processes giving rise to the spectrum-to-spectrum variations. An introduction to PCA is given in Francis and Wills of this volume, where our present dataset is used as an example.

We choose some of the same variables as in §3.1, and perform the analysis on the ranks of the measurements for each observational variable. The results are shown in Table 2². Half of the sample variance (49.9%) is described by a linear combination of variables related to the optical–X-ray principal component PC1

²For the results of a PCA on the unranked data, see Table 3, of Francis and Wills in this volume).

Table 2. Principal Components Analysis

	PC1	PC2	PC3
Eigenvalue	6.49	2.47	1.63
Proportion	0.499	0.190	0.126
Cumulative	0.499	0.689	0.815
Variable	PC1	PC2	PC3
L_{1216}	+0.01	+0.52	-0.30
α_x	+0.32	-0.16	+0.03
FWHM $H\beta$	-0.35	+0.03	-0.32
Fe II/ $H\beta$	+0.35	-0.09	+0.09
EW [O III]	-0.30	+0.02	+0.25
FWHM C III]	-0.20	-0.06	-0.61
EW Ly α	-0.15	-0.51	+0.10
EW C IV	-0.33	-0.24	+0.05
C IV/Ly α	-0.34	+0.18	+0.03
EW C III]	-0.25	-0.47	-0.08
Si III]/C III]	+0.35	-0.06	-0.02
N V/Ly α	+0.23	-0.14	-0.54
$\lambda 1400$ /Ly α	+0.23	-0.31	-0.24

There were 18 QSOs used in this analysis. L_{1216} represents continuum luminosity at 1216Å.

found by Boroson & Green (1992) and Laor *et al.* (1994, 1997a). The weights of these measured parameters are given in the PC1 column.

The second most important principal component (PC2) is dominated by an inverse relationship between L_{1216} and EW. All EWs except EW $H\beta$, EW [O III], and EW Fe II(optical) show likely inverse relationships between EW and luminosity, and the correlation appears particularly strong for O VI $\lambda 1034$ (not shown; see the results of Zheng *et al.* 1995, for a large heterogeneous sample.) These are the same trends as seen in the classical Baldwin relationships (Kinney *et al.* 1990). The most interesting result of the PCA is that PC1 appears not to depend on luminosity at all (correlation coefficient ~ 0.1): The Baldwin relationships appear independent of the X-ray–UV–optical PC1 relationships. C IV $\lambda 1549$ is present in PC1 and PC2, probably accounting for its weaker Baldwin relationship in our sample (Fig. 3).

PC3 appears to represent an independent relationship between luminosity and line widths, but we defer consideration of this until a larger sample is available. Each of the remaining principal components account for less than 5% of the sample variance and are not significant.

4. Summary

We show that optical principal component 1, linking steeper soft X-ray spectra with increasing optical Fe II strength, decreasing [O III] $\lambda 5007$ emission, and nar-

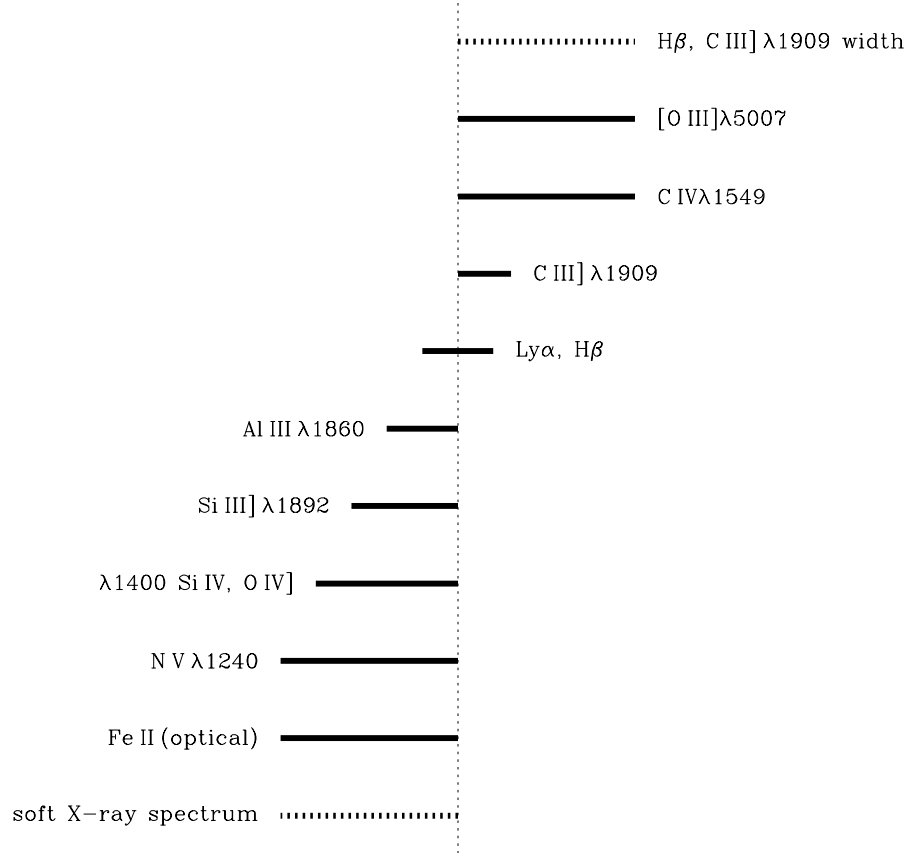


Figure 4. An approximate description of the relationships among α_x , UV PC1 variables, and optical PC1 variables. Variables on the same side of the center correlate positively with each other, and on opposite sides, negatively. The lengths of the bars indicate an approximate strength of the correlation.

rower BLR H β emission, extends to the UV emission lines: narrower C III]λ1909, weaker C IVλ1549 emission, stronger low ionization emission lines – UV Fe II, Si III]λ1892, and probably O Iλ1305, C IIλ1335, and Fe III, and also a larger ratio Si III]λ1892/C III]λ1909. But N V and the O IV–Si IV λ1400 blend also increase in strength with steeper soft X-ray spectrum, increasing Fe II(optical), decreasing H β width and decreasing [O III] strength. Figure 4 presents an approximate summary of these correlations and anticorrelations, based on the results for many line ratios.

While Fe II(optical) vs. λ1400/C IV and C IV/Ly α , and α (UV–X-ray) vs. C IV/Ly α relationships have been noted before in large, heterogeneous samples (Wang et al. 1996, 1998; see also Dultzin-Hacyan 1997), the spectacular related correlations that we have found among many variables may be attributed to the homogeneous and complete nature of the sample. For further illustration and discussion of the Fe II – Si III]/C III] relationships, as well as AlIII/C III]

and Fe III/C III], see Aoki & Yoshida (this volume), and for an independent presentation of the C IV – [O III] relationship, see Brotherton (this volume).

5. Discussion

In the Introduction, we showed that the X-ray–optical relationships provide plausible strong links between central engine parameters and ionized gas on sub-parsec to Kpc scales. Clearly the UV–soft-Xray continuum photoionizes the surrounding gas and the emission lines can, in principle, provide information on the shape of the ionizing continuum. *UV spectrophotometry* provides further pieces for the puzzle by relating the central engine to the kinematics, geometry and density of fueling gas or outflows:

- $\text{Si III}]\lambda 1892$ probably arises from almost the same region as C III] and most optical and UV Fe II, but $\text{C III}]\lambda 1909$ is collisionally suppressed at high densities $>10^{10} \text{ cm}^{-3}$, thus increasing the ratio $\text{Si III}/\text{C III}]$ (e.g. Laor *et al.* 1997b). Our observed dependence of $\text{Si III}]/\text{C III}]$ on Fe II strength is therefore consistent with the high densities and column densities required to produce strong Fe II(optical) (Ferland & Persson 1989, Wills, Netzer & Wills 1985).
- The C IV emission is strongly correlated with $[\text{O III}]\lambda 5007$. As suggested to explain the inverse Fe II-[OIII] relation, does this mean that thick high density Fe II-emitting gas shields more distant C IV-emitting gas?
- The strength of the higher-ionization $\text{N V}\lambda 1240$ also appears to be associated with this higher density gas, while C IV strength decreases with increasing PC1 (i.e., Fe II, etc.) This apparent anomaly is reminiscent of the behavior of the EW(N V) Baldwin relation in which the slope of the Baldwin relation for several other species is tightly correlated with ionization potential, but for N V the dependence on luminosity is much less than expected. Korista *et al.* (this volume, 1998) show that the EW (N V) – luminosity relationship can be understood if very N-rich gas (Hamann & Ferland 1993) is irradiated by a UV–soft-Xray continuum whose strength increases with luminosity. While this is a complex issue, perhaps our N V anomaly can be similarly explained by enhanced N abundances.

The ‘mystery physics’ underlying the PC1 relationships could be an increase in L/L_{Edd} associated with an increase in dense, Fe II emitting gas of high metallicity. It has been suggested that the extreme low ionization spectra with strong Fe II are somehow related to starbursts (Lipari *et al.* 1993). Could starburst activity cause high accretion rates, hence strong soft X-rays?

What do our new results mean for the Baldwin Effect? Our PCA suggests that the strong first principal component (PC1) relationships that we find are independent of luminosity. The second principal component, PC2, apparently represents the Baldwin effect – inverse relationships between EW and luminosity. Because we find strong links among line strengths and UV–X-ray continuum parameters, it is clear that these relationships must cause significant variation in equivalent widths from one QSO to another. Even if their cause is unknown, the relationships between line strengths and observables independent of L could be used to remove most of the scatter in Baldwin relationships. Could the cause of PC1 remove not only the scatter from the Baldwin relationships, but also remove the Baldwin effect itself? Not if PC1 is independent of luminosity; investigation of larger samples is needed. However, if the variance of emission-

line strengths could be attributed entirely to differences in the ionizing spectral energy distribution, the crucial question would then become: How and why does the ionizing spectral energy distribution depend on luminosity?, and this gets to the heart of the Central Engine.

Acknowledgments. We gratefully acknowledge the help of C. D. Keyes & A. Roman of STScI, and M. Dahlem (now of ESTEC), also M. Cornell and R. Wilhelm who provide computer support in the Astronomy Department of the University of Texas. This research is supported by NASA through LTSA grant number NAG5-3431 (B.J.W.) and grant number GO-06781 from the Space Telescope Science Institute, which is operated by the Association of Universities for Research in Astronomy, Inc., under NASA contract NAS5-26555.

References

Baldwin, J. A., Burke, W. L., Gaskell, C. M., Wampler, E. J. 1978, *Nature*, 273, 431

Baldwin, J. A., Ferland, G. J., Korista, K., & Verner, D. 1995, *ApJ*, 455, L119

Boroson, T.D. & Green, R.F. 1992, *ApJS*, 80, 109

Dultzin-Hacyan, D. 1997, in IAU Colloquium 159: Emission Lines in Active Galaxies: New Methods & Techniques, eds. B.M. Peterson, F.-Z. Cheng, & A.S. Wilson, ASP Conf. Ser. 113, 262

Ferland, G.J. & Persson, S.E. 1989, *ApJ*, 347, 656

Francis, P. J., Hewett, P. C., Foltz, C. B., & Chaffee, F. H. 1992, *ApJ*, 398, 476

Grupe, D., Beuermann, K., Mannheim, K. & Thomas, H.-C. 1998, *A&A*, submitted

Hamann, F., & Ferland, G.J. 1993, *ApJ*, 418, 11

Kinney, A. L., Rivolo, A. R., & Koratkar, A. P. 1990, *ApJ*, 357, 338

Korista, K., Ferland, G.J., & Baldwin, J.A. 1997, *ApJ*, 487, 555

Korista, K., Baldwin, J., & Ferland, G.J. 1998, *ApJ*, in press

Laor, A. 1998, *ApJ*, 505, 83L

Laor, A., Fiore, F., Elvis, M., Wilkes, B., & McDowell, J.C. 1994, *ApJ*, 435, 611

Laor, A., Fiore, F., Elvis, M., Wilkes, B., & McDowell, J.C. 1997a, *ApJ*, 477, 93

Laor, A., Jannuzzi, B. T., Green, R. F., Boroson, T. A. 1997b, *ApJ*, 489, 656

Lipari, S., Terlevich, R., Macchetto, F. 1993, *ApJ*, 406, 451

Netzer, H. 1985, *ApJ*, 289, 451

Peterson, B. M., Wanders, I., Bertram, R., Hunley, J. F., Pogge, R. W., Wagner, R. M. 1998, *ApJ*, 501, 82

Pounds, K. A., Done, C., & Osborne, J. P. 1995, *MNRAS*, 277, L5

Wang, T.-G., Zhou, Y.-Y., & Gao, A.-S. 1996, *ApJ*, 457, 111

Wang, T.-G., Lu, Y.-J., & Zhou, Y.-Y. 1998, *ApJ*, 493, 1

Wills, B.J., Laor, A., Wilkes, B.J., et al. 1998a, in Structure & Kinematics of Quasar Broad Line Regions, ed. Gaskell, C. M. et al. (ASP Conf. Ser.), in press

Wills, B.J., Laor, A., Wilkes, B.J., et al. 1998b, in preparation
Wills, B.J., Netzer, H., & Wills, D. 1985, *ApJ*, 288, 94
Zheng, W., Kriss, G.A., & Davidsen, A.F. 1995, *ApJ*, 400, 606